Production and deexcitation of highly deformed ^{67}Ga

Z. Majka,* M. E. Brandan,† D. Fabris, K. Hagel, A. Menchaca-Rocha,† J. B. Natowitz, G. Nebbia, G. Prete,‡ B. Sterling, and G. Viesti§

Cyclotron Institute, Texas A&M University, College Station, Texas 77843

(Received 23 December 1986)

The energy spectra and angular distributions of alpha particles and protons emitted from ^{67}Ga compound nuclei at excitation energies of 110 to 116 MeV formed in four different reactions have been measured. The populated angular momentum ranges deduced from fusion cross section information correspond to $0-24\hbar$ for ^{4}He+^{63}Cu, $0-38\hbar$ for ^{12}C+^{55}Mn, $0-48\hbar$ for ^{16}O+^{51}V, and $0-50\hbar$ for ^{40}Ar+^{27}Al. The experimental data are analyzed using the angular-momentum-dependent statistical model and the rotating liquid drop model. Average multiplicities and barriers are extracted for different zones of angular momentum. Comparisons with the models indicate large deformations of the ^{67}Ga nuclei at the higher angular momenta and suggest large deformation related increases in the nuclear level density and decreases of emission barriers. The p/α ratio decreases with increasing angular momentum less than expected for spherical emitters at the higher angular momenta. The average α emission barriers are found to be close to those which are calculated for emission from the tips of prolate deformed nuclei such as those predicted by the liquid drop model. The experimental proton barriers appear somewhat smaller than those calculated using the liquid drop model shapes.

I. INTRODUCTION

The sizes and/or shapes of composite nuclei with very large angular momenta and high excitation energies are largely unknown. One of the most interesting predictions of several theoretical treatments[1] of rapidly rotating nuclei is the expectation of large deformations. Searches for experimental evidence of such deformed nuclei has caused intense research activity in this subject area during the last few years.

Heavy ion projectiles can deliver very large amounts of angular momentum and energy into reacting systems. The subsequent deexcitation of the product nuclei may involve fission, evaporation of nucleons or clusters, and γ-ray emission. The rates of evaporation are related to the level densities of emitting and residual nuclei and the evaporation Coulomb barriers. Both quantities can be strongly affected if the nucleus under consideration becomes deformed. The use of light charged evaporated particles as probes to explore the shape of the emitting nucleus has been explored by several groups.[2-5]

Alexander and co-workers[2] analyzed a large set of mean energies and angular anisotropies for evaporative α-particle emission to obtain evaporation barriers, B. The difference between the empirical s-wave fusion barrier, E, and B, is interpreted as an indication of the extent of distortion of the α emitters. The analysis of the evaporation barrier suggests that as Z increases from ≈ 35 to ≈ 100 the deformation parameter for a spheroid, α_{20}, used to characterize the system, increases from ≈ 0 to 0.6. For nuclei $Z > 70$, rather extended shapes were inferred, even for emitters of a rather low spin.

The measurements with the spin spectrometer of angular distributions of evaporated α particles with respect to the spin directions of residual nuclei from fusion of 176 MeV ^{20}Ne with ^{150}Nd have been reported recently.[3] The spin spectrometer,[6] a 4π γ-ray multidetector system, provides a sensitive method for determining the magnitude and orientation of the spin of the residual nucleus on an event-by-event basis. Near the Coulomb barrier, the ratio of the in plane to out of plane yield, with respect to spin direction, increases with decreasing alpha particle energy. Comparison of these results with statistical model calculations enabled the authors to come to the conclusion that the α-emitting nuclei are deformed with their longest axis perpendicular to the spin direction.

The α-particle spectra in coincidence with residues of ^{59}Cu nuclei produced in the fusion of 214 MeV ^{32}S with ^{27}Al have been measured by Choudhury *et al.*[4] The observed deviations at both high and low particle energies of the experimental spectra from the spectra calculated using the statistical model for spherical nuclei suggest large angular momentum induced deformation.

In this work we have followed the well established strategy[7] of forming the same compound nucleus at the same excitation energy through several entrance channels. For different choices of entrance channel the angular momentum distributions of the compound nuclei differ. The evaporation properties of several localized regions of angular momentum were determined by comparison of the deexcitation properties of the resultant compound nuclei.

The experimental details of the present measurements are given in Sec. II and results are presented in Sec. III. The general features of our statistical model calculations and resulting properties of the hot highly rotating ^{67}Ga nucleus are discussed in Sec. IV. The conclusions of the present work are summarized in Sec. V.

II. EXPERIMENTAL METHODS

Four different beams, listed in Table I, from the Texas A&M variable energy cyclotron, were used to bombard appropriate targets to produce ^{67}Ga compound nuclei at 110–116 MeV excitation energy. The Mn target was on a 68 μg/cm^2 carbon backing. Other targets were self-supporting. Thicknesses are listed in Table I. The detection system is sketched in Fig. 1. For each reaction, light particles, H and He, were observed with two three-member Si telescopes (20, 250, and 5000 μm). The silicon detectors were calibrated by normalizing a pulser to the peak due to the 5.48 MeV α-particle decay of ^{241}Am. A large position sensitive four anode ionization chamber telescope[8] (LIC) was used to detect evaporation residues and other heavy reaction products. The LIC was connected to the 43 cm scattering chamber through an intermediate box so that the LIC window was approximately 120 cm from the target. The LIC was positioned at a mean angle of 20° with respect to the beam and with its large solid angle was able to detect heavy reaction products over a range of ±10° in the reaction plane and ±3° out of the reaction plane. The in plane angular calibration was obtained from measurements of the geometry of this detector and by fitting a position spectrum for the elastic scattering of ^{40}Ar from ^{197}Au to the calculated Rutherford scattering distributions. The energy calibrations were established by using a range-energy table, a pulser normalized to the peak of the 5.48 MeV α-particle decay of ^{241}Am, and the elastic scattering of ^{40}Ar from ^{27}Al and ^{197}Au. For the ^{40}Ar + ^{27}Al reaction the light particles were measured in coincidence with heavy reaction products detected by the ionization chamber. A large Bragg curve spectrometer[9] (BCS) with a position sensitive parallel plate avalanche counter mounted in front was also used to detect the heavy reaction products. A supplementary experiment was carried out in a 76 cm diam ORTEC chamber. In this latter experiment the absolute calibration of the Faraday integrator and the zero of the angular scale were obtained by fitting angular distributions of the elastic scattering of each beam from ^{197}Au to the calculated Rutherford cross sections. Measured differential cross sections for particle emission were normalized to the elastic scattering to obtain absolute cross sections. Additionally, we measured for each beam the production of H and He from a carbon target to estimate contributions to the light particle spectra resulting from carbon impurities in each target.

TABLE I. Reaction parameters. The limits adopted for the calculations are estimated from empirical systematics of fusion cross sections as well as model calculations. See, for example, J. R. Birkelund, L. E. Tubbs, J. R. Huizenga, J. N. De, and D. Sperber [Phys. Rep. **56**, 107 (1979)] and W. W. Wilcke, J. R. Birkelund, H. J. Wollersheim, A. D. Hoover, J. R. Huizenga, W. W. Schroder, and L. E. Tubbs [At. Data Nucl. Data Tables **25**, 391 (1980)]. Estimated uncertainties are ±5%.

Projectile	Target {thickness (mg/cm^2)}	E_{lab} (MeV)	E^* (MeV)	l_{cr} ($\hbar$)
^{4}He	^{63}Cu {0.4}	120	116	24
^{12}C	^{55}Mn {0.25}	130	116	38
^{16}O	^{51}V {0.6}	133	110	48
^{40}Ar	^{27}Al {0.5}	240	110	50

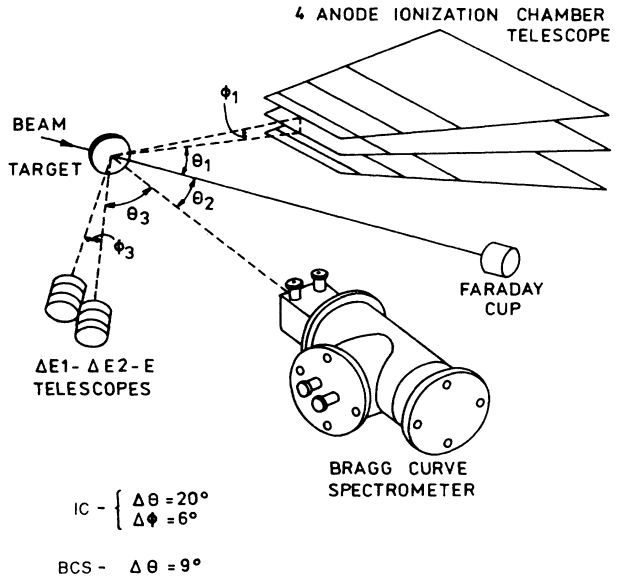

FIG. 1. Schematic design of the experimental setup. Ionization chamber (IC) and Bragg curve spectrometer (BCS) acceptable angles are indicated.

Data were recorded event by event on magnetic tape with a VAX 11/780 computer. The computer code LISA (Ref. 10) was used to extract energy spectra of the light particles and the heavy ions as well as the various experimental correlations.

To close this section, we emphasize again that the experimental data presented in this analysis were taken in one experimental run where four different projectile beams were used. Thus the measured particle spectra are derived from a single consistent energy calibration.

III. EXPERIMENTAL RESULTS

Energy spectra in the laboratory frame for the reactions under consideration are given in Figs. 2–5 for ^{4}He and in Figs. 6 and 7 for two selected reactions for ^{1}H. The main features to note from these figures are the narrow evaporative-like shapes of the laboratory spectra at backward angles for ^{4}He + ^{63}Cu, ^{12}C + ^{55}Mn, and ^{16}O + ^{51}V reactions.

The ^{40}Ar + ^{27}Al measurements taken with the so called "inverse" kinematics display large kinematic shifts with angle and the evaporative emission is focused into the forward hemisphere. An overall view of the emission pattern for "normal" and "inverse" kinematics can be clarified using contour polar plots of the invariant cross section in velocity space for detected particles. As can be seen in Fig. 8, the symmetric emission from a thermally equilibrated compound nucleus moving with a velocity designated $V_{c.m.}$ is observed in the backward hemisphere for the reaction ^{4}He + ^{63}Cu and in the forward hemisphere for the reaction ^{40}Ar + ^{27}Al. The solid arcs drawn with

centers at the tip of the $V_{c.m.}$ vector have a radius very close to the Coulomb velocities of α particles in the decay $^{67}Ga \rightarrow {}^{63}Cu + {}^{4}He$. Figure 8(b) also shows the advantage of the "inverse kinematics" for the reduction of the effective detection threshold at the forward angles.

As noted, the targets, except for the Mn target, which was carbon backed, were self-supporting. From fragment fragment coincidence measurements using these targets and a C target of 199 $\mu g/cm^2$ thickness, we were able to evaluate the maximum C contamination of the targets. The maximum contribution to the particle spectra in the angular ranges of primary interest, i.e., forward in the $^{40}Ar + {}^{27}Al$ case and backward in the other cases, was found, except for the Mn case, to be always $\lesssim 6\%$. For the $^{40}Ar + {}^{27}Al$ case, the upper limit was 3%. Effects on the spectral shape were negligible. Because of the carbon backing and the relative thinness of the Mn target, the contribution was found to be 30% at back angles. The forward angle data for Mn are heavily contaminated by the carbon contribution, as can be seen in Fig. 3. The differential cross sections and subsequent multiplicities of particle emission have been corrected for carbon contamination.

Figure 9(a) presents the two dimensional plot $\Delta E1$-E_{tot}

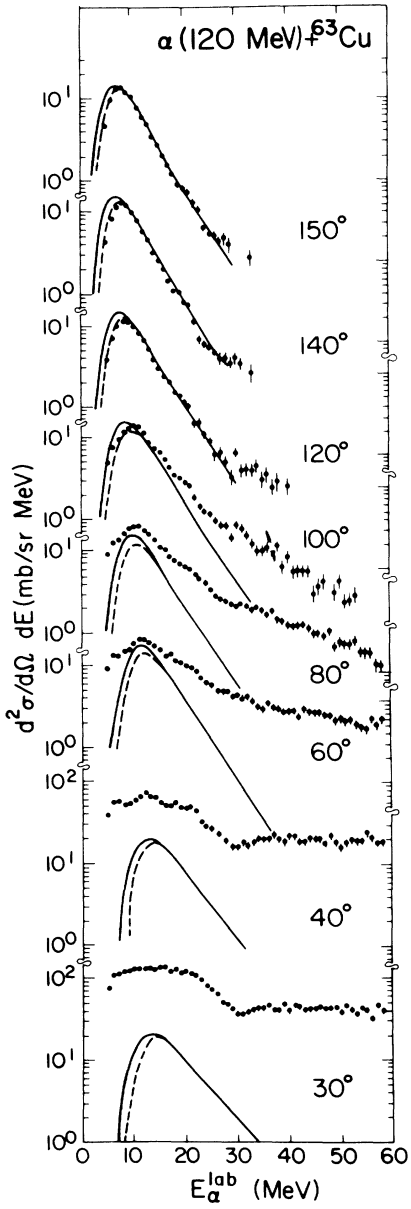

FIG. 2. Experimental laboratory energy spectra for ^{4}He (points with statistical errors are shown) for the reaction $^{4}He + {}^{63}Cu$ compared to calculated curves from the statistical model evaporation theory; dashed line represents the calculation where an evaporation barrier was taken from the inverse reaction (Ref. 22), and a moment of inertia is that for the spherical nucleus; the solid line represents a calculation where the evaporation barrier was lowered and the moment of inertia was increased (see text).

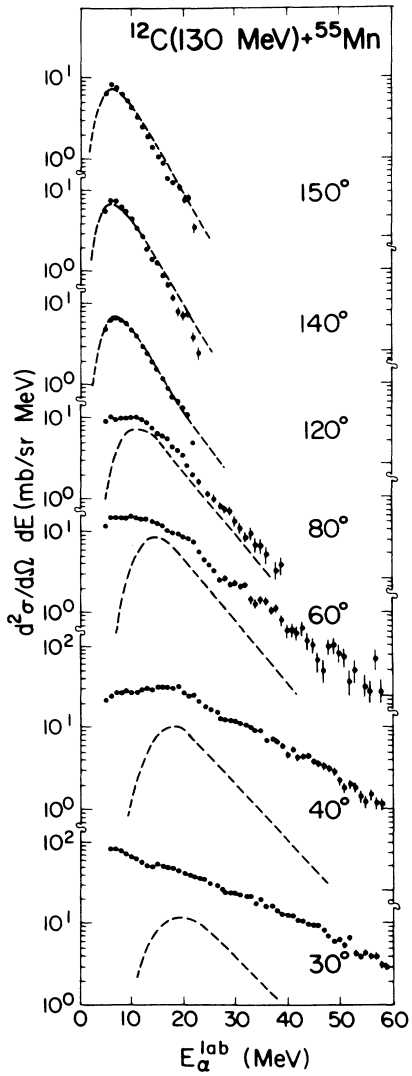

FIG. 3. Same as Fig. 2, but for the reaction $^{12}C + {}^{55}Mn$.

of the heavy reaction products for the reaction $^{40}Ar + ^{27}Al$ detected in the large ionization chamber (plotting this picture, we selected $\theta_{res} = 12.1° \pm 1.1°$). Products with $\Delta E1$ and E_{tot} inside the dashed line contour were identified as evaporation residues following fusion. The energy spectrum of the residues is presented in Fig.

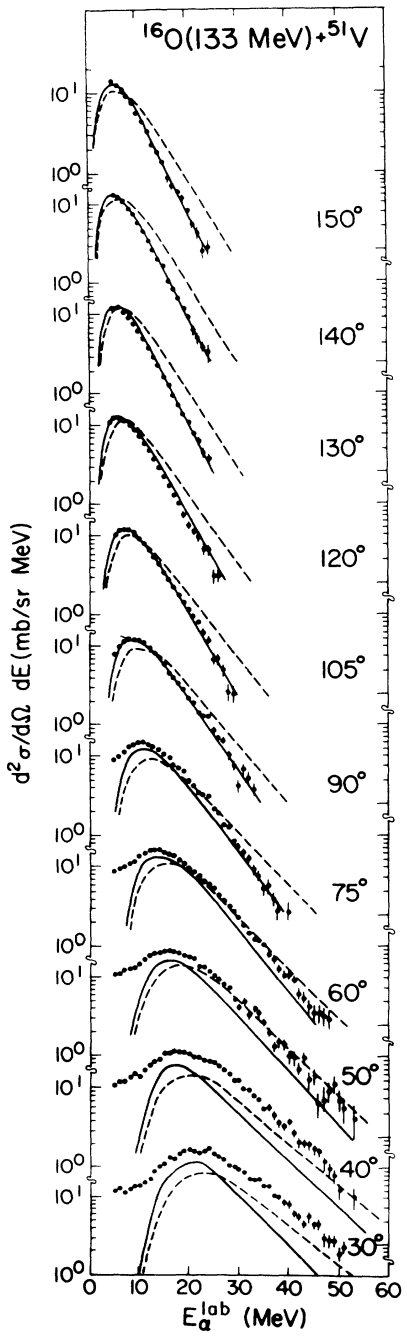

FIG. 4. Same as Fig. 2, but for $^{16}O + ^{51}V$.

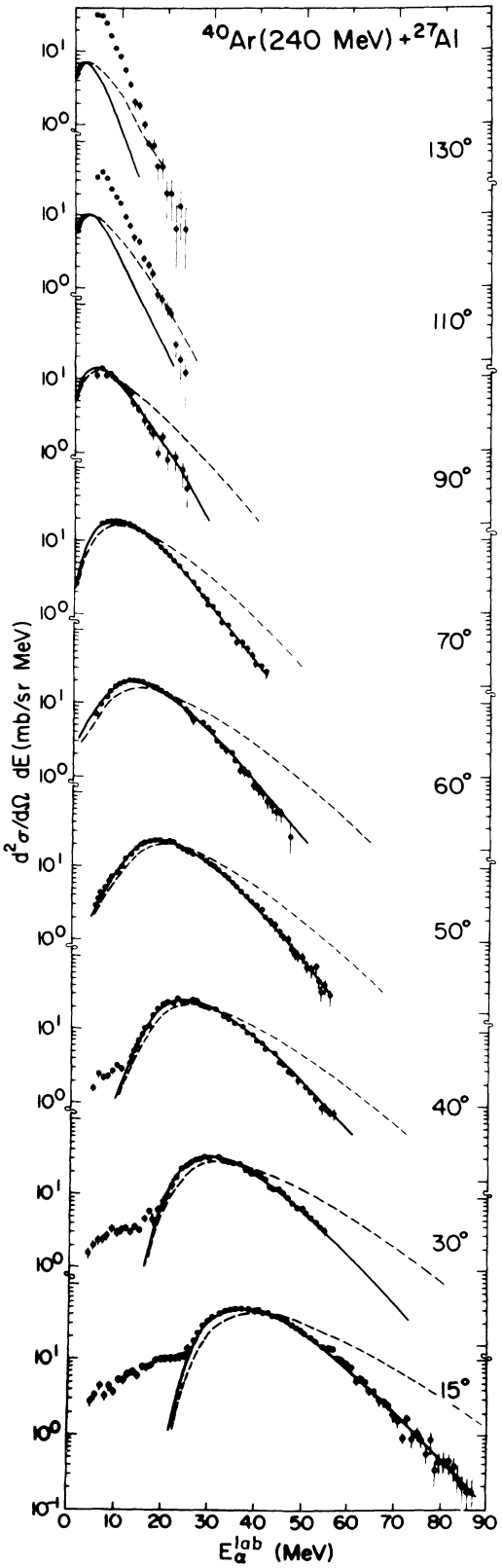

FIG. 5. Same as Fig. 4, but for $^{40}Ar + ^{27}Al$.

10. To show our Z resolution for this detector we present additionally a $\Delta E2$-E_{tot} plot in Fig. 9(b) (reaction products which pass through the two forward anodes). Elastically scattered ^{40}Ar projectiles from the ^{27}Al target nucleus are located at the upper part of Figs. 9(a) and 9(b).

For the inverse kinematics the angular distribution of evaporation residues drops rapidly with angle (4 orders of magnitude from 10° to 20°), having a very small counting rate at 20°. Coincident H and He energy spectra were obtained at several forward angles on the opposite side of the beam from the residue detector.

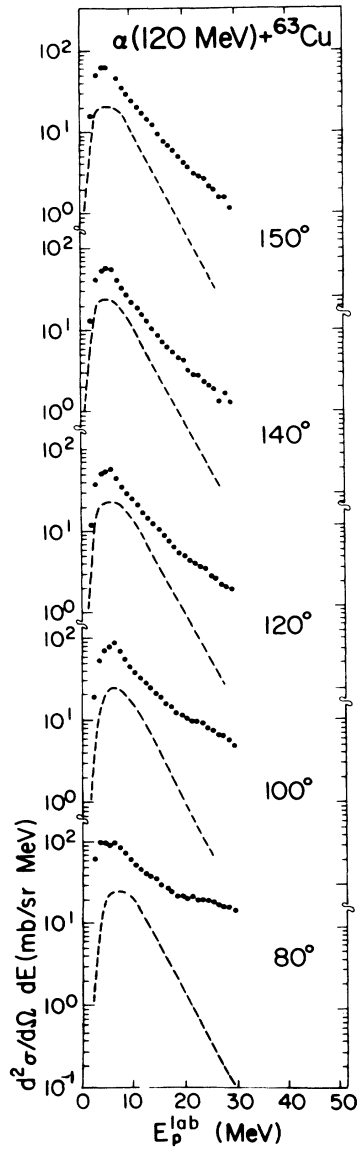

FIG. 6. Experimental laboratory energy spectra for ^{1}H (points with statistical errors are shown) in the reaction of ^{4}He + ^{63}Cu compared to calculated curve from the statistical model evaporation theory with the parameter set for spherical compound system.

Figure 11 shows a comparison of the experimental alpha particle energy spectra collected in the inclusive and exclusive modes for the ^{40}Ar + ^{27}Al reaction. At low energies a contribution from deeexcitation of deep inelastic reaction products may be seen. This contribution is also apparent in the backward angle velocity spectra of Fig. 8

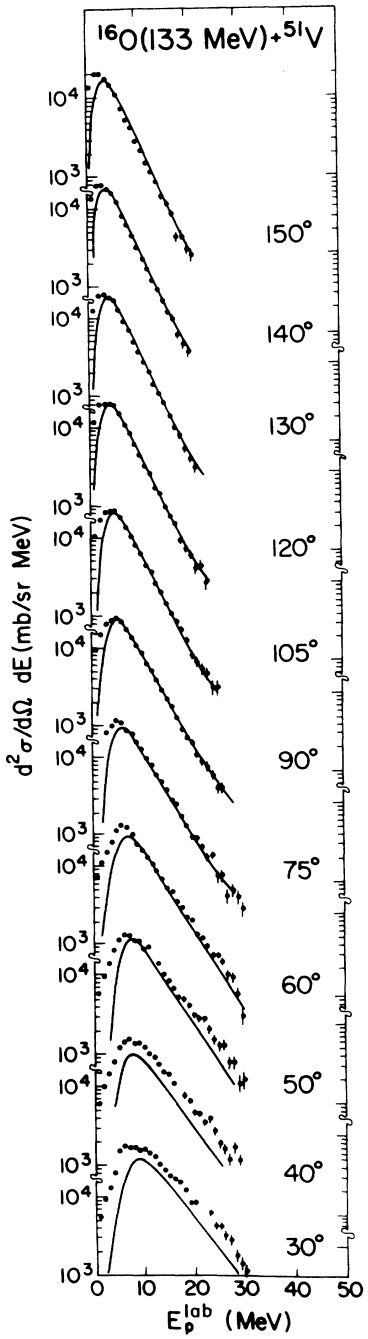

FIG. 7. Same as Fig. 6, but for the reaction ^{16}O + ^{51}V. The calculated curves are with a lowered evaporation barrier and increased moment of inertia consistent with the parameter set derived from α-emission spectra.

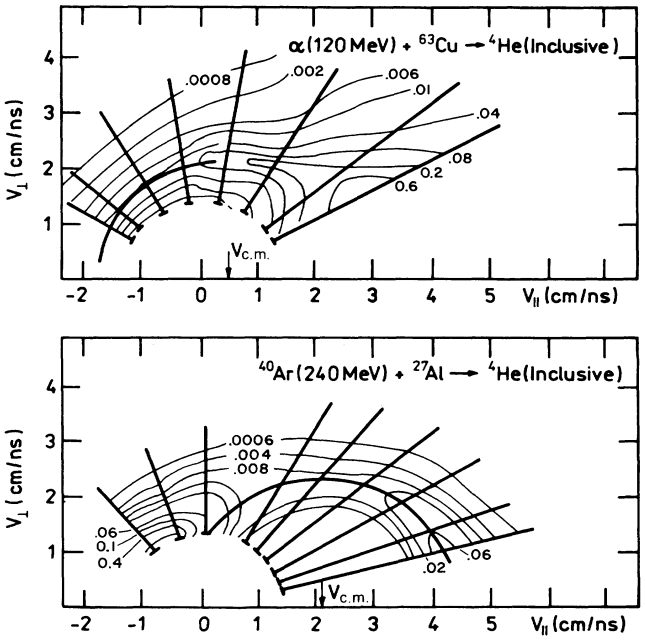

FIG. 8. Contour plot of the cross section $d^3\sigma/dv^3$ as a function of the velocity of alpha particles. The vectors $V_{c.m.}$ indicate the velocity of the ^{67}Ga compound nucleus. The axes $V_{||}$ and $V_{\perp}$ denote laboratory velocity components parallel and perpendicular to the beam, respectively. The solid circular arcs are centered on $V_{c.m.}$. The lines radiating from 0 indicate the angles at which data were taken and the thresholds for detection.

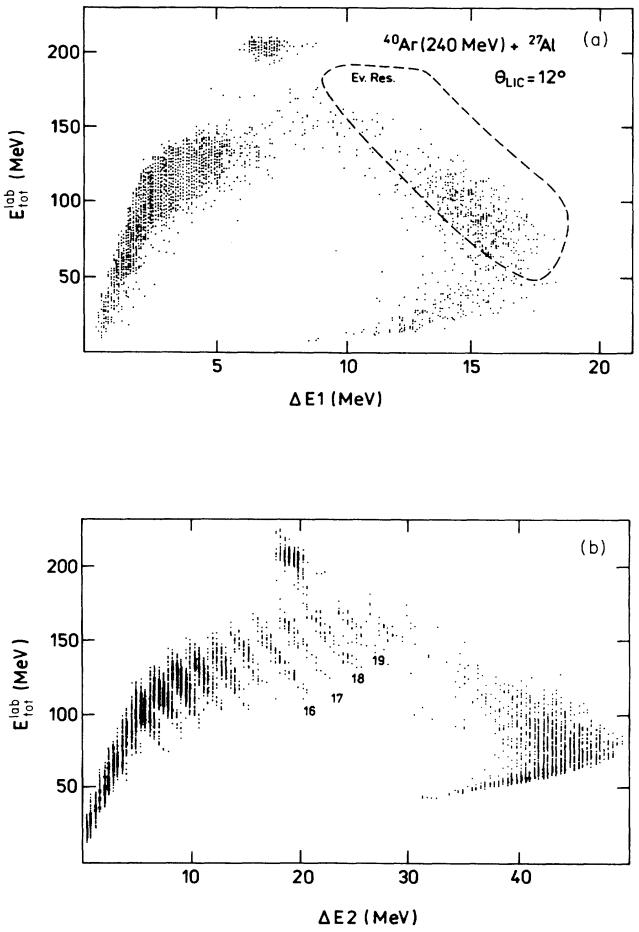

FIG. 9. Two dimensional plots of the heavy reaction products in the large ionization chamber: (a) energy loss $\Delta E1$ (first anode) vs E, total energy; (b) energy loss $\Delta E2$ (second anode) vs E, total energy.

when the contribution from residues is greatly suppressed. From the coincidence experiments, we estimate that the contribution to the singles spectrum is less than 10% at the most forward angles. The shapes of the exclusive spectra in which the deep inelastic component is substantially reduced are consistent with the calculated shapes represented by the solid lines in Fig. 5. That the deep inelastic component is not totally removed results from the fact that a small fraction of the products from such reactions falls in the residue window indicated in Fig. 9(a).

IV. DISCUSSION

A. Statistical emission

The importance of the angular momentum in the evaporation of particles from compound nuclei has been discussed in many theoretical papers (see, e.g., Refs. 11—13 and references quoted therein). Angular momentum dependent statistical model calculations show that the probabilities of α-particle emission and the average energy of the emitted α particles are strongly affected by angular momentum.[12,13] In these calculations the emission spectra of protons and neutrons are less strongly affected.

The statistical model expresses the shape of the evaporation spectrum for the emission of the particle ν with the energy ϵ from the compound nucleus formed by the projectile x as

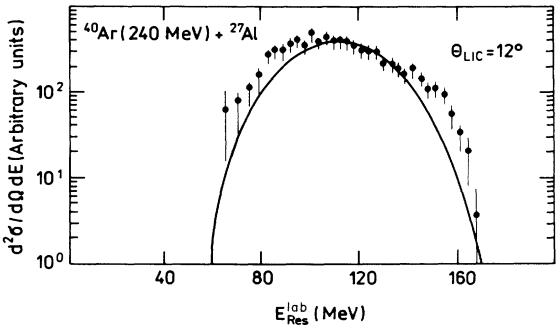

FIG. 10. Experimental energy spectra for evaporation residues (points with statistical errors are shown) compared to the statistical model calculation (solid line).

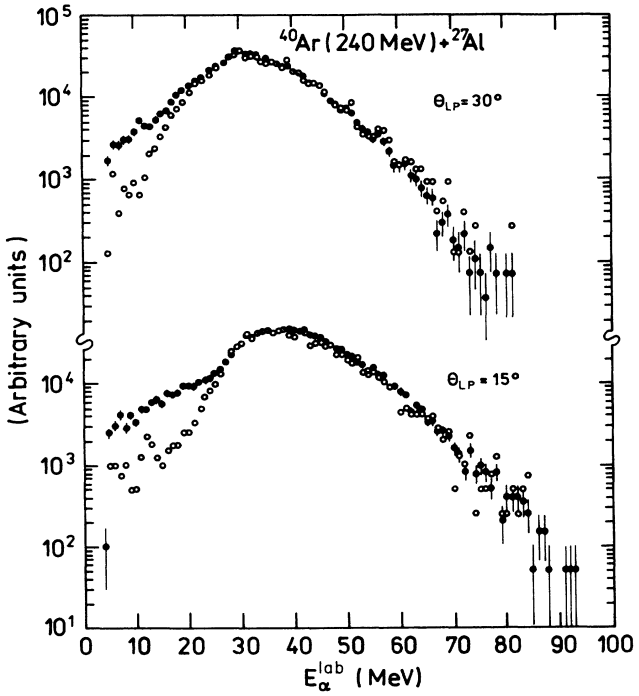

FIG. 11. Alpha particle energy spectra for the reaction of ^{40}Ar with ^{27}Al; singles (solid points) and coincidence with evaporation residues (open circles). Evaporation residues were detected at 12° on the opposite side of the beam from the light particle detector. The light particle telescope angles, θ_{LP}, are indicated.

$$\frac{d\sigma(x,\nu)}{d\epsilon} = \sum_{J=0}^{\infty} \sigma_J(x) P_J(\nu,\epsilon) , \tag{1}$$

where $\sigma_J(x)$ is the cross section for the formation of the compound nucleus with angular momentum J. The probability $P_J(\nu,\epsilon)$ for the emission of the particle with energy ϵ from the compound nucleus with the angular momentum J is proportional to the cross section in the inverse process and expressed as the product of the level density in the daughter nucleus $\rho_f(E_f,J_f)$ and transmission coefficient

$$P_J(\nu,\epsilon) \simeq \rho_f(E_f,J_f) T_J^{\nu}(\epsilon) . \tag{2}$$

The decay of the compound nucleus is independent of the formation, except for the conservation of mass, charge, energy, angular momentum, etc. It is assumed that the compound nucleus lives long enough before the emission to randomize its motion in all degrees of freedom. Both quantities on the right-hand side of the expression (2) are strongly dependent on the possible deformation of the daughter nucleus. The transmission coefficients $T_J(\epsilon)$ are derived from the inverse process, i.e., the reaction between an incoming particle ν and the excited daughter nucleus. However, the reaction between projectiles and target nuclei can be investigated experimentally only in their ground states and the transmission coefficients are derived from standard optical model potentials for elastic scattering. Note that in the sharp cutoff approximation the classical transmission coefficient for a completely absorptive nucleus of radius R_{SA} is

$$T_J^{\nu}(\epsilon) = \begin{cases} 0 \text{ for } \epsilon < B_C + \dfrac{\hbar^2 J(J+1)}{2\mu R_{SA}} , \\ 1 \text{ for } \epsilon \geq B_C + \dfrac{\hbar^2 J(J+1)}{2\mu R_{SA}} , \end{cases} \tag{3}$$

where μ is a reduced mass. The angular momentum dependence of the transmission coefficient is seen to be contained in the centrifugal potential and also in the Coulomb barrier B_C as a result of the angular momentum induced deformation.[1]

In order to estimate the expected changes of the Coulomb barrier between the evaporated particle and the deformed daughter nucleus, we modified a semimicroscopic folding model[14] for a deformed system. The effective potential (nuclear plus Coulomb) between the alpha particle and the ^{63}Cu nucleus is calculated in the form

$$V_{\alpha\text{-Cu}}(r,\beta) = 2\pi \int\int dz\, dR \rho_m(\mathbf{R},\mathbf{z},\beta) V_{\alpha\text{-N}}(\rho_m, |\mathbf{R}+\mathbf{z}-\mathbf{r}|) + 4\pi \int\int dz\, dR \rho_{ch}(\mathbf{R},\mathbf{z},\beta) \frac{1}{|\mathbf{R}+\mathbf{z}-\mathbf{r}|} , \tag{4}$$

where the coordinates are defined in the inset of Fig. 12 and β stands for a parameter set of the deformation. The density dependent alpha particle—bound nucleon effective interaction, $V_{\alpha\text{-N}}$, was taken from Ref. 15. Assuming

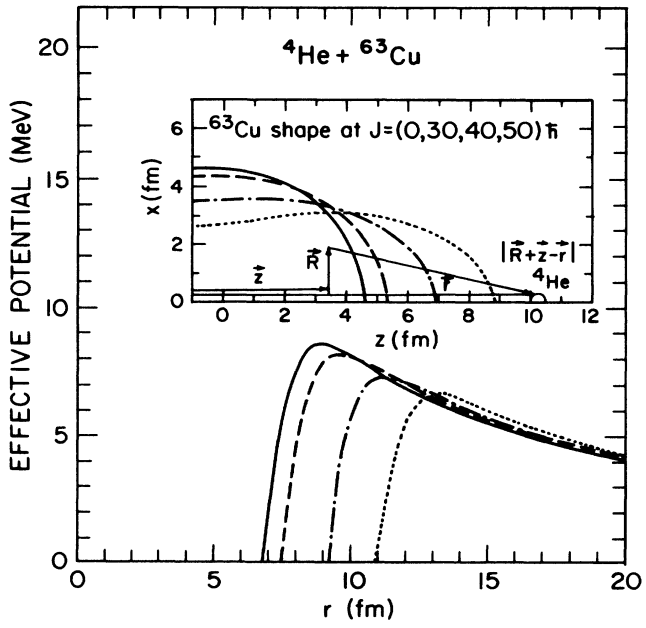

FIG. 12. Effective ^{4}He-^{63}Cu potential calculated using Eq. (4) for different deformations of the ^{63}Cu nucleus. A schematic sketch of the coordinates used in Eq. (4) is presented in the inset. Shapes of ^{63}Cu and potential curves for emission from the tips are shown for 0$\hbar$ (solid line), 30$\hbar$ (dashed line), 40$\hbar$ (dotted-dashed line), and 50$\hbar$ (dotted line).

TABLE II. Evaporation barriers.

System	Fusion barrier[a] $l=0$	Statistical model[b] $l=0$	Adjusted statistical model[c] $l=0$	Microscopic calculations[d] at $J=$ 0	30	40	50
^{63}Cu + ^{4}He	8.9	9.1	8.4	8.7	8.2	7.4	6.6
^{66}Zn + ^{1}H	5.0	4.5	3.8	5.1	4.7	4.4	3.9

[a]From formulae of Ref. 28. For emission from ^{67}Ga.
[b]Effective barriers ($T_0=0.5$) for emission from ^{67}Ga from optical model transmission coefficient calculation with standard parameters.
[c]Effective barriers ($T_0=0.5$) for emission from ^{67}Ga required to fit low energy portions of spectra for ^{40}Ar and ^{16}O entrance channels (see text).
[d]Barriers for emission from tips of prolate shapes calculated by the LDM (see text, Figs. 12 and 13).

that the proton and matter distributions are identical, a two-parameter Fermi shape is used to describe the matter, ρ_m (charge, ρ_{ch}) point density distribution for the spherical ^{63}Cu nucleus. These distributions are extracted from the measured charge density distribution by unfolding the charge density distribution of a single proton.[16] Contours of constant matter (charge) density with deformation were described using the parametrization of Mustafa *et al.*[17]

In Fig. 12 we present the effective alpha particle—^{63}Cu nucleus potentials calculated from Eq. (4) for emission from the tips for a few selected shapes of the ^{63}Cu nucleus. These shapes correspond to the equilibrium configurations of ^{63}Cu nuclei obtained from the finite range, two center, rotating liquid drop model developed by Mustafa and co-workers[17,24] and calculated at angular momenta of 0, 30, 40, and 50$\hbar$. As can be seen in Fig. 13, the Coulomb barrier decreases with increasing deformation and at $J=40\hbar$, when the ^{63}Cu becomes superdeformed (the ratio of a minor to major semiaxes is equal to 1:2), the Coulomb barrier is lowered by 1.3 MeV, as compared to the value of the spherical nucleus (see Table II). In Fig. 13 results of a similar calculation for p + ^{66}Zn are depicted.

The level density entering expression (2) is a crucial quantity for the statistical decay and has been discussed by many authors (see, e.g., Refs. 11 and 18–20). The angular momentum dependent level density formula for a spherical nucleus as given by Lang[18] is

$$\rho(E^*,J)=\frac{1}{24}\sqrt{2}(1/a)^{1/4}\frac{1}{\sigma^3}\frac{2J+1}{E^{*5/4}}$$
$$\times\exp\{2[a(E^*-(J+\tfrac{1}{2})^2\hbar^2/2\mathscr{I})]^{1/2}\}\ , \quad (5)$$

where σ and a are the spin cutoff parameter and level density parameter, respectively, $\mathscr{I}$ is the nuclear moment of inertia, and E^* is the excitation energy. Thus, in the spherical case, E^* is reduced by the energy tied up in rotational energy. The moment of inertia increases dramatically if the ^{67}Ga nucleus becomes superdeformed. In addition, significant amounts of energy can be tied up in the collective deformation. For the deformed nucleus, E^* must be reduced by a yrast energy which accounts for these changes. As a result, deformation can greatly affect the level density.

B. Emission from spherical nuclei

As a first step of our analysis, we tested the adequacy of the statistical model representation and established the basic parameters of the calculation by a comparison with the alpha particle spectral data for the ^{4}He + ^{63}Cu reaction. The calculations were performed using the CACARIZO code, which is a Monte Carlo version of the CASCADE code.[21] In this program a single compound nucleus is created with a certain angular momentum and the deexcitation path is followed and recorded as an event in a file. These events are then analyzed using a different code in which one can specify the locations and solid angles of the detectors. This program allows for the determination of the types of events singles, coincidence, etc. to be sorted

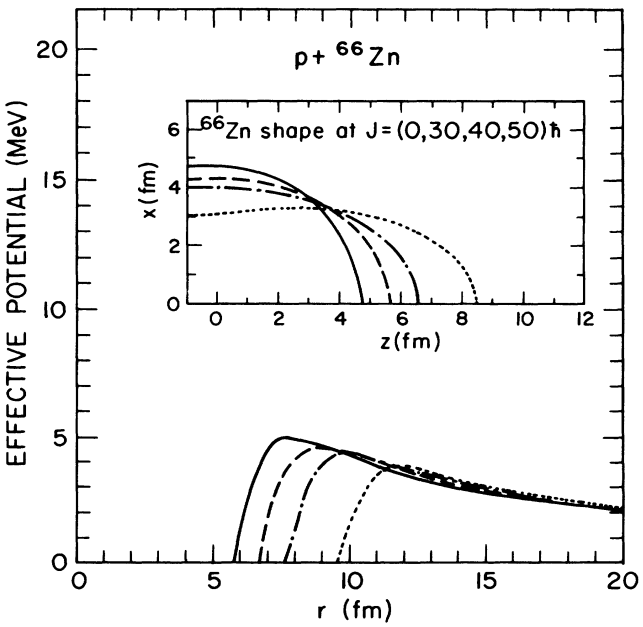

FIG. 13. Effective ^{1}H-^{66}Zn potential calculated for different deformations of the ^{66}Zn nucleus. Shapes of ^{66}Zn and potential curves for emission from the tips, calculated for angular momenta of 0, 30, 40, and 50$\hbar$, are shown. The line convention is the same as Fig. 12.

and the spectra to be created.

The probabilities for the various modes of decay of the compound nucleus are determined by the statistical weights of the final states and the transmission coefficients from the initial to the final states. The transmission coefficients are calculated from optical model potentials.[22] The level densities at higher excitation energies are calculated from the formula given by Eq. (5).[18] At low excitation energies, the level density parameters are determined from a parametrization of the results of Dilg *et al.*,[23] assuming that $\mathcal{I}=0.85\mathcal{I}_{\text{rigid}}$. Odd-even effects are included. The γ emission is treated as in Ref. 21, assuming reduced widths for $E1$, $M1$, and $E2$ radiation of 0.001, 0.05, and 5 W.u., respectively. As can be seen in Fig. 2, the experimental evaporation spectra for emission of ^{4}He in the ^{4}He + ^{63}Cu reaction are well reproduced at the more backward angles (dashed lines) by the model calculation under the assumption that the evaporation takes place from a spherical nucleus.

At the ^{4}He energy of 30 MeV/nucleon chosen to match compound nucleus excitation energies, the projectile velocity is such that the most probable momentum transfer and therefore the average recoil velocity and average excitation energy of the composite nucleus are slightly less than those of the compound nucleus. We have used the statistical model calculations to estimate the effect of the less than total momentum transfer. The emission barriers derived from the experimental spectra and reported later in this section have been corrected for this effect. Using the same parameter set as for the ^{4}He + ^{63}Cu system, the statistical model calculations reproduce also the alpha particle energy spectra for the ^{12}C + ^{58}Mn reaction, at the backward angles where clear evaporation spectra are observed (dashed lines in Fig. 3). In particular, the high energy portions of the spectra (sensitive to the yrast line) are well fitted. The total spectrum appears adequately fitted, although the high experimental threshold in the backward spectra might mask some barrier lowering.

In contrast, for the ^{16}O + ^{51}V and ^{40}Ar + ^{27}Al reactions the experimental spectra disagree with the spherical calculation in both the low and high energy parts (see Figs. 4 and 5, dashed lines).

In order to clarify this observation, we present in Fig. 14 the energy—angular momentum (E-J) plane for the ^{67}Ga compound nucleus studied in this paper. The equilibrium yrast shapes depicted for different angular momenta J of the rotating nucleus were calculated using codes provided by Mustafa.[17,24]

Four collective yrast lines are also shown in Fig. 14. The dashed line represents the yrast line (rotational energy) for a spherical ^{67}Ga nucleus. The dotted-dashed line represents the yrast line (rotational and deformation energy) calculated for the equilibrium deformations of the Mustafa model.[17,24] The dotted lines represent yrast lines used in this work and discussed below.

The heavy solid lines near the top of the Fig. 14 indicate the excitation energies and the angular momentum ranges (assuming the sharp cutoff limits of Table I) for the compound nuclei formed in each of the different reactions. It is seen that for the two reactions ^{16}O + ^{51}V and ^{40}Ar + ^{27}Al the compound system is produced with angular momenta for which strong prolate deformations are predicted. Thus disagreement between the observed and calculated spectra for these two reactions may well be the result of deformation effects.

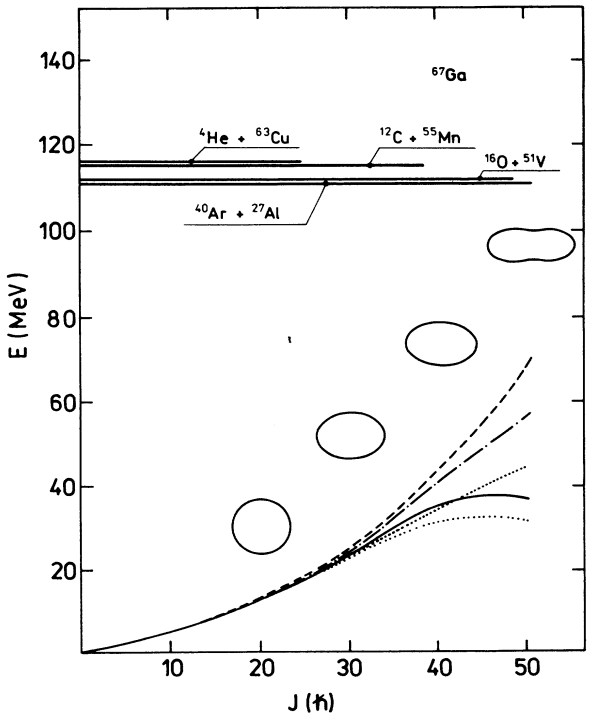

FIG. 14. Collective energy lines for ^{67}Ga in the E-J plane. The long-dashed line represents the yrast line of a spherical ^{67}Ga nucleus. The dashed-dotted line represents the yrast line (rotational and deformation energies) for ^{67}Ga nuclei with angular momentum dependent shapes predicted by the model of Ref. 17. The solid line represents only the rotational energy corresponding to the shapes in Ref. 17. The lower dotted line is the empirical yrast line required to fit the experimental particle spectra (see text). The heavy horizontal lines near the top of the figure indicate the excitation energies and angular momentum ranges for fusion in the different entrance channels assuming the sharp cutoff limits of Table I.

C. Deformation simulation

Following the discussion in the earlier part of this section, we have attempted to simulate deformation effects in the statistical model calculation by the following:

(a) Modification of the optical model potential parameter to change the evaporation barrier.

(b) Changes of the moment of inertia of the compound system to modify the nuclear level densities.

As can be seen in Fig. 15, if the effective emission barrier is lowered by increasing the optical potential radius as compared to the normally assumed radius, the calculated cross section for the low energy part of the alpha particle spectrum increases (compare the dashed and dotted-dashed lines in Fig. 15). Changing the yrast line by increasing the moment of inertia of the system, we observed

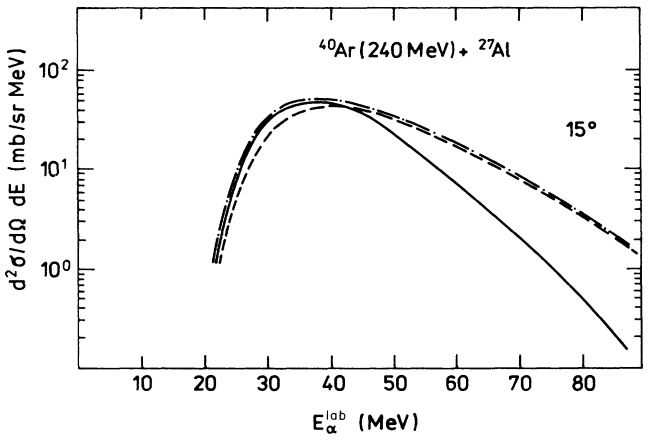

FIG. 15. Effect of parameter modification on calculated alpha particle energy spectra. Evaporation barrier and moment of inertia for the spherical nucleus (dashed line), evaporation barrier lowered 1.5 MeV (dotted-dashed line), and evaporation barrier lowered and moment of inertia increased (solid line).

the high energy part of the alpha spectrum to be lowered (solid line).

The evaluation of the nuclear level densities for the deformed nucleus is a very complicated task and still far from being in a completely satisfactory form. The main effects of the deformation which have to be included in the nuclear density formula are the following:[19,20]

(1) The moment of inertia of the deformed system changes as compared to the moment of inertia of the spherical nucleus.

(2) For different nuclear shapes different portions of the total excitation energy E^* are tied up in the deformation energy, $E_{\rm def}$, and rotational energy, E_R, i.e., the yrast line changes as a function of deformation.

(3) A collective enhancement of the nuclear level densities for the deformed nucleus is expected.

This complicated modification of the level density was approximated in our statistical model calculations through the use of angular momentum dependent moment of inertia in the form

$$\mathscr{I}=\mathscr{I}_{\rm sph}(1+\delta_1 J^2+\delta_2 J^4)\ , \tag{6}$$

to calculate the energy of the yrast line. The first estimations for the parameters δ_1 and δ_2 were obtained by a least squares fit of the yrast line obtained using the Mustafa model (dotted-dashed line in Fig. 14). Note, however, that for the level density calculation of formula (5), the moment of inertia of the spherical nucleus was retained in the preexponential spin cutoff term.

A complete search of the statistical model deformation dependent parameters is a formidable task. However, it was possible to reproduce the experimental alpha particle spectra with the evaporation statistical model calculation for the ^{16}O + ^{51}V and ^{40}Ar + ^{27}Al reactions (Figs. 4 and 5, solid line) by gradually adjusting the evaporation barrier and the position of the yrast line. The necessary modifications were the following:

(1) The evaporation barrier was lowered from the value 9.1 MeV, which was appropriate for the earlier two reactions ^{4}He + ^{63}Cu and ^{12}C + ^{55}Mn to the value 8.4 MeV. The earlier value can be compared to the empirical fusion barrier 8.9 MeV for the reaction ^{4}He + ^{63}Cu obtained by McMahan and Alexander.[25] The fact that these values are very close indicates that for the ^{4}He + ^{63}Cu and ^{12}C + ^{55}Mn reactions evaporation of the alpha particles takes place from the spherical nucleus. On the other hand, the lower evaporation barrier required for the ^{16}O + ^{51}V and ^{40}Ar + ^{27}Al reactions suggests that in these cases the evaporation takes place from an extended evaporating nucleus.

(2) The angular momentum dependent moment of inertia (6) was modified in such a way that the yrast energy line used in the calculations (lower dotted line in Fig. 14) was somewhat below that of the yrast line resulting from the Mustafa model and surprisingly close to the line representing only rotational energy. Since the bulk of the α emission is not first step, the yrast line is most uncertain at the very highest angular momenta. The two empirical yrast lines represented in the figure give acceptable fits to the shapes of the energy spectra. The lower one provides the better fit over the entire angular range and is the one used.

If we apply the modified parameter set to the ^{4}He + Cu reaction, the statistical model calculations overpredict the alpha emission at low energies (solid line in Fig. 2). The high energy portions of these spectra are not affected because for that reaction the higher values of the spin are not populated and the compound system does not change its moment of inertia significantly.

We emphasize that the agreement between the calculation and the data was obtained by using an effective or "statistical" yrast line which at the higher angular momenta is significantly below the collective energy yrast line calculated using the finite range liquid drop model (LDM) with diffuseness. This statistical yrast line turns out to be lower than the line corresponding to the Mustafa LDM calculation of the collective energy. Conceptually, this approach may be viewed as a progressive lowering of the rotating ground state with increasing angular momentum (deformation), which is required to increase the effective excitation energy and thus the level density at the excitation energies sampled in the evaporation. In this sense, it is analogous to the commonly used procedure of displacing the nuclear ground state to account for odd-even changes in the level density relative to a reference odd A nucleus as a result of pairing effects. The result of the yrast line lowering is such that, for a particular excitation energy, the decrease in level density with increasing J is slower than would be calculated using a level density built from the LDM yrast line according to Eq. (5). An alternative approach to adjusting the level density would be to fix the yrast line at the LDM values and define a progressively increasing level density parameter, a_J, with increasing angular momentum. In such an approach, changes of $\approx 25\%$ in a_J would be required as the angular momentum increased from 0 to 50$\hbar$.

The energy spectra for the protons are presented in Figs. 6 and 7 for the ^{4}He + ^{63}Cu and ^{16}O + ^{51}V reactions, respectively. The statistical model calculations represented in these figures by the dashed and solid lines were performed using the same parameter set as for the alpha particles already discussed. It is apparent from Fig. 6 that the statistical model calculations for the ^{4}He + Cu reactions underestimate the experimental proton energy spectra by a factor of almost 2 in the backward hemisphere where the evaporation spectra are expected to dominate. This effect can be understood taking into consideration that the ^{4}He + ^{63}Cu reaction was measured at the energy 30 MeV/nucleon. For a very similar system, it was shown by Budzanowski *et al.*[26] that the proton evaporation spectra are considerably contaminated by processes other than complete fusion. The same is not true for the α spectra. The results for H evaporation for the ^{16}O + ^{51}V reaction shown in Fig. 7 present another interesting feature. Even though the evaporation barrier was modified in the same way as for the alpha particles, the statistical model predictions still underestimate the low energy parts of the evaporation spectra. Agreement would require the further reduction of the evaporation barrier (see Table II), which would not agree with apparent shape deformation for alpha emission. A similar observation was reported recently by Moses *et al.*[27]

D. Emission from specific zones of J

More information on the evolution of the ^{67}Ga nucleus shape can be obtained by studying the particles emitted from the high angular momentum zones of the compound nucleus. The cross section for the formation of the compound nucleus with angular momentum J can be expressed as

$$\sigma_J(x)=\pi\lambda\!\!\!^{-2}_x(2J+1)T_J(x)\ , \tag{7}$$

where $\lambda\!\!\!^{-}$ is the reduced wavelength in the entrance channel and $T_J(x)$ is the transmission coefficient for the formation of the compound nucleus with angular momentum J by projectile x. Substituting this expression into Eq. (1) and using the resulting equation for two different entrance channels, one can get[7]

$$\frac{d\sigma(x_1,\nu)/d\epsilon}{\pi\lambda\!\!\!^{-2}_{x_1}}-\frac{d\sigma(x_2,\nu)/d\epsilon}{\pi\lambda\!\!\!^{-2}_{x_2}} = \sum_{J=0}^{\infty}(2J+1)P_J(\nu,\epsilon)[T_J(x_1)-T_J(x_2)]\ . \tag{8}$$

The expression in the square brackets on the right-hand side of Eq. (8) is nonzero only when the transmission coefficients $T_J(x_1)$ and $T_J(x_2)$ have different values. The transmission coefficient changes its value from 1 for the lower values of the angular momenta to 0 for the higher ones in the vicinity of the critical value of the angular momentum J_{cr}. The left-hand side of Eq. (8) consists only of experimental differential cross sections and entrance channel wave lengths.

In Fig. 16 the energy spectra of the emitted alpha particles from the high angular momentum regions (solid and dashed lines) of the ^{67}Ga nucleus are shown together with the calculated energy spectra in the center of mass for all four reactions (open symbol). The angular momentum dependent alpha particle spectra for $J>24\hbar$ were obtained when the calculated differential cross section $(d\sigma/d\epsilon)/\pi\lambda\!\!\!^{-2}_\alpha$ obtained for the reaction induced by the alpha particle (bottom of figure) was subtracted from the calculated differential cross section $(d\sigma/d\epsilon)/\pi\lambda\!\!\!^{-2}_x$ obtained for the other three reactions (x stands for ^{12}C, ^{16}O, and ^{40}Ar projectiles, respectively). The resulting difference spectra are represented by the dashed line in Fig. 16.

The solid line for $J>38\hbar$ was obtained when the $(d\sigma/d\epsilon)/\pi\lambda\!\!\!^{-2}_{^{12}C}$ spectrum was subtracted from the spectra for the ^{16}O + ^{51}V and ^{40}Ar + ^{27}Al reactions, respectively. This procedure assumes that calculated total energy spectra in the center of mass system are equivalent to the ex-

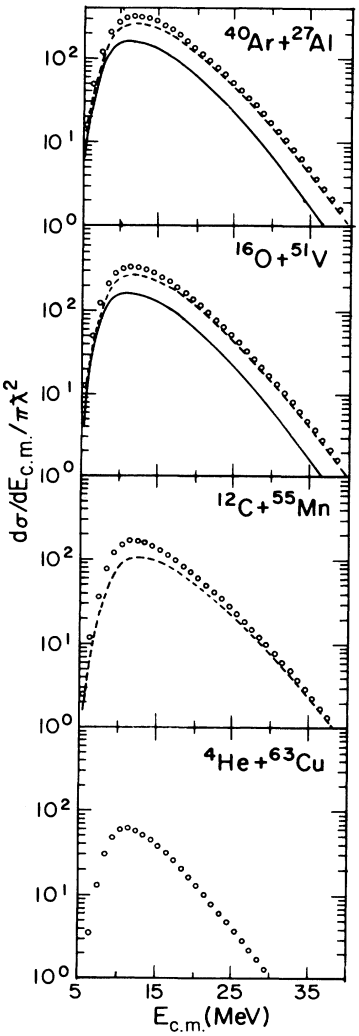

FIG. 16. Energy spectra in the center of mass reference frame for emitted alpha particles resulting from the statistical model calculation and normalized (see text). The center of mass spectra for four different entrance channels are indicated. The lines represent the energy spectra of emitted alpha particles from the high angular momentum zones. The dashed lines represent spectra for $J\geq 25\hbar$, the solid lines $J\geq 39\hbar$.

perimental ones because the experimental spectra in the laboratory system are well reproduced by the calculated spectra. In this way we are able to avoid the difficulties of transformation of the experimental data to the center of mass system and errors connected with the angle integration of the spectra and with the energy threshold.

Subtraction of the α spectrum from the $^{4}He + ^{63}Cu$ reaction from those observed in other reactions gives spectra (dashed lines) corresponding to the emission from higher angular momenta zones in ^{67}Ga. One can see that the evaporation of the alpha particles from the low angular momentum zone ($0 \leq J \leq 24$) represents a small fraction of the evaporation observed from the same nucleus under a higher rotation. This considerable enhancement of emission of α particles from higher angular momentum zones is particularly apparent in Table III, where multiplicities of evaporated alpha particles and protons from different angular momentum zones are given.

The solid lines in Fig. 16 represent the evaporation of the alpha particles from the angular momentum range $(39 \leq J \leq 50)\hbar$ for the $^{40}Ar + ^{27}Al$ reaction and $39-48\hbar$ for the $^{16}O + ^{51}V$ reaction. The most probable energy of these spectra is 2–3 MeV lower than the peak energies of the full spectra.

The exact value of the barriers cannot be ascertained from these spectral subtractions since the barriers used in the calculations are weighted average barriers over the entire spectra. However, the weighted average barrier appropriate to a particular angular momentum range can be determined using the cross sections and average multiplicities for different angular momentum zones together with the weighted average barriers which have been deduced for particular entrance channels.

For example, the average α multiplicity for the $0-38\hbar$ zone is found to be 1.22, while that for the $39-50\hbar$ zone is found to be 1.80. For the former zone the weighted average barrier B_α is 9.1 MeV. For the entire $0-50\hbar$ range the weighted average barrier is 8.4 MeV. Thus, following the sharp cutoff approximation, the barrier appropriate to the $38-50\hbar$ zone is simply related to these,

$$\bar{B}_{II} = \frac{\bar{B}_{I,II}(\sigma_I M_I + \sigma_{II} M_{II}) - \sigma_I M_I \bar{B}_I}{\sigma_{II} M_{II}} , \quad (9)$$

where B, σ, and M represent the barrier, cross section, and multiplicity appropriate to angular momentum zones I ($0-38\hbar$), II ($39-50\hbar$), or I and II ($0-50\hbar$). This approach may, of course, be applied to other combinations of angular momentum zones. The barriers appropriate to the different angular momentum zones are presented in Table III.

TABLE III. Angular momentum dependent multiplicities and barriers.

Reaction	Angular momentum zone ($\hbar$)	Multiplicity ^{4}He	Multiplicity ^{1}H	Average B_α (MeV)
$^{4}He + ^{63}Cu$	0–24	0.87	2.45	9.1
$^{12}C + ^{55}Mn$	0–38	1.22	2.09	9.1
$^{16}O + ^{51}V$	0–48	1.45	1.55	8.4
$^{40}Ar + ^{27}Al$	0–50	1.46	1.53	8.4
	25–38	1.45	1.85	9.1
	25–50	1.63	1.27	8.3
	39–50	1.80	0.77	7.6

Since the spherical barrier appropriate to our experiments, 9.1 MeV, is slightly higher than the 8.9 MeV calculated using the methods of Ref. 28, we compare the experimental and calculated barriers in Fig. 17 in terms of the fractional barrier relative to that of a spherical nucleus. It is clear from this figure that the data indicate a progressive lowering of the barrier with increasing angular momenta, in very good agreement with the model predictions for the barriers at the tips of deformed nuclei as described in Sec. IV A. Since the calculated barriers are for emission from the tips of prolate spheroids, the experimental results suggest that such emission is indeed dominant in the high angular momentum range.

Although the high energy portions of the proton spectra are well fitted by the yrast line derived from the α particle data, the experimental proton spectra have a surplus of low energy protons when the barrier parameters appropriate to the same average deformations as used for α particles are applied (see Fig. 7). A natural explanation for this might be a greater sensitivity of proton emission to the more highly deformed shapes. Certainly, dropping the yrast line from the spherical line enhances the proton to alpha emission ratio in the statistical model calculation, but this enhancement does not appear to be sufficient to explain the discrepancy, given the absolute multiplicities of Table III. In addition, in Fig. 18 it will be noted that reducing the barrier from the value of 4.4 MeV (consistent

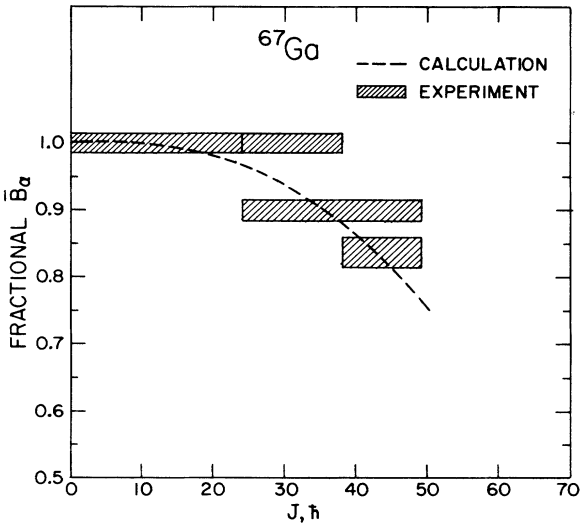

FIG. 17. Experimental and calculated barriers as a function of the ^{67}Ga angular momentum. The fractional barriers relative to that for a spherical nucleus are shown. The bars represent experimental determinations for the angular momentum zones represented. Vertical widths correspond to estimated errors. The dashed line corresponds to the α-barrier calculation shown in Fig. 13.

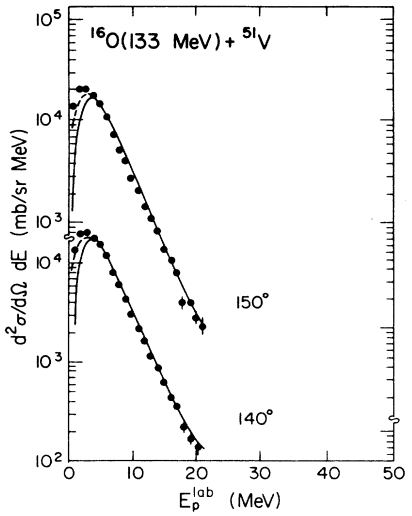

FIG. 18. Spectral fits for protons emitted following the $^{16}O + {}^{51}V$ reaction. The dashed line indicates the improved fit if the proton barrier for the most deformed nuclei predicted by model calculations for $J = 50\hbar$ is used.

with the α-particle parametrization) to 3.7 MeV (approximately consistent with the largest deformations expected from the liquid drop model for $J = 50\hbar$) improves the agreement but does not yet account for all the low energy protons. A further reduction to values far below the calculated values would be required, suggesting the necessity for extraordinary deformations. Alternatively stated, applying the same techniques as embodied in Eq. (9) to determine the proton barrier appropriate to the highest angular momentum zone would lead to proton barriers much lower than those for the LDM shapes. It has been suggested that such barriers might result from nucleon emission from an expanded nuclear surface region prior to complete equilibration of the compound nucleus.[29]

V. SUMMARY AND CONCLUSIONS

Through comparisons of experimental measurements and model calculations of the proton and α-particle emission from ^{67}Ga compound nuclei produced in fusion reactions employing four different entrance channels, the particle multiplicities and emission barriers for different initial angular momentum zones have been determined.

With increasing angular momentum the multiplicity of α emission increases while the proton multiplicity decreases. The p/α ratio does not decrease as rapidly as predicted for spherical emitters in the same angular momentum range. The emission of α particles from ^{67}Ga compound nuclei of varying angular momenta is characterized by barriers and yrast lines which imply increasing nuclear deformations with increasing angular momentum. The experimental barriers, in particular, are in good agreement with barriers calculated for the emission from the tips of prolate nuclei with deformations calculated using the liquid drop model. This suggests that emission from the tips of the prolate deformed shapes may be dominant at high angular momentum. If that were not the case, interpretation of these barriers as weighted average barriers over a deformed nucleus (prolate or oblate) would demand deformations much larger than those predicted by the liquid drop model. The statistical yrast lines required to fit the high energy portions of the spectra are even lower than those calculated using the LDM, suggesting that there may be a deformation related enhancement of the level density which is simulated in this calculation by the yrast line lowering. Accepting the LDM yrast line as valid, a comparable softening of the calculated spectra could be achieved by progressively increasing the level density parameter with increasing deformation. Increases of some 25% would be required as J increases.

When the same shapes are assumed in calculating the proton emission spectra, it is found that the high energy, yrast-line-sensitive portions of the spectra are well fitted by the same yrast line required for the modeling of the α-particle spectra. In contrast, proton barriers consistent with the shape parametrizations which model the α-particle barriers are found to be not low enough to reproduce the low energy portions of the proton emission spectra. Fitting these spectra at low energies with the standard form of the statistical model would require very low proton emission barriers, well below the barriers expected for the most deformed nuclei predicted by the liquid drop model for the angular momenta expected.

ACKNOWLEDGMENTS

This research was supported by the U.S. Department of Energy, the Robert A. Welch Foundation, and the Istituto Nazionale di Fisica Nucleare. Two of us (M.E.B.) and (A.M.) appreciate the financial support of the Fondo Nacional de Ciencias, Conicyt, Chile, for travel associated with this research. Another of us (Z.M.) thanks the Cyclotron Institute, Texas A&M University, for the kind hospitality, and the CPBP 01.09 program for partial financial support. We thank J. M. Alexander, M. Kaplan, and M. G. Mustafa for valuable discussions during the progress of this research.

---

*On leave from the Institute of Physics, Jagellonian University, Cracow, Poland.

†Permanent address: Instituto de Fisica, Universidad Nacional Autónoma de México, Apartado Postal 20-364 01000 México, Distrito Federal, México, and Facultad de Ciencias, Universidad de Chile, Santiago, Chile.

‡Permanent address: Istituto Nazionale di Fisica Nucleare, Laboratori Nazionali di Legnaro, Legnaro (Padova), Italy.

§Permanent address: Istituto Nazionale di Fisica Nucleare and Dipartimento di Fisica dell'Universita di Padova, Padova, Italy.

[1]S. Cohen, F. Plasil, and W. J. Swiateki, Ann. Phys. (N.Y.) 82,

557 (1974); T. Bengtsson, M. Faber, M. Ploszajczak, I. Ragnarsson, and S. Åberg, Lund University report, 1983.
[2]J. M. Alexander, D. Guerreau, and L. C. Vaz, Z. Phys. A **305**, 313 (1982).
[3]F. A. Dilmanian, D. G. Sarantites, M. Jaaskelainen, H. Puchta, R. Woodward, J. R. Beene, D. C. Hensley, M. L. Halbert, and R. Novotny, Phys. Rev. Lett. **49**, 1909 (1982).
[4]R. K. Choudhury, P. L. Gonthier, K. Hagel, M. N. Namboodiri, J. B. Natowitz, L. Adler, S. Simon, S. Kniffen, and G. Berkowitz, Phys. Lett. **143B**, 74 (1984).
[5]M. Blann and T. T. Komoto, Phys. Rev. C **24**, 426 (1981).
[6]D. G. Sarantites, J. Phys. (Paris) Colloq. **41**, C10-269 (1980); D. G. Sarantites, R. Lovett, and R. Woodward, Nucl. Instrum. Methods **171**, 503 (1980).
[7]R. C. Reedy, M. J. Fluss, G. F. Herzog, L. Kowalski, and J. M. Miller, Phys. Rev. **188**, 1771 (1969).
[8]H. Sann, H. Damjantschitsch, D. Hebbard, J. Junge, D. Pelte, B. Povh, D. Schwalm, and D. B. Tran Thoai, Nucl. Instrum. Methods **124**, 509 (1974); M. N. Namboodiri, J. B. Natowitz, R. Patton, K. Hagel, W. Chapman, D. Crocker, H. O'Neill, F. Abegglen, and L. Duel, Progress in Research 1980–1981, Cyclotron Institute Report, Texas A&M University, p. 76.
[9]A. Moroni, I. Iori, L. Z. Yu, G. Prete, G. Viesti, F. Gramegna, and A. Dainelli, Nucl. Instrum. Methods **225**, 57 (1984).
[10]W. Kuhn, private communication.
[11]T. Dossing, Niels Bohr Institute Report, 1978 (unpublished).
[12]T. Ericson, Adv. Phys. **9**, 423 (1960).
[13]M. Blann, Phys. Rev. C **21**, 1770 (1980).
[14]Z. Majka, A. Budzanowski, K. Grotowski, and A. Strzalkowski, Phys. Rev. C **18**, 114 (1978).
[15]H. J. Gils, E. Friedman, Z. Majka, and H. Rebel, Phys. Rev. C **21**, 1245 (1980).
[16]R. F. Frosch, R. Hofstadter, J. S. McCarthy, G. K. Noldeke, K. J. van Oostrum, M. R. Yearian, B. C. Clark, R. Herman, and D. G. Rawenhall, Phys. Rev. **174**, 1380 (1978).
[17]M. G. Mustafa and P. A. Baisden, and H. Chandra, Phys. Rev. C **25**, 2524 (1982).
[18]D. W. Lang, Nucl. Phys. **77**, 545 (1966).
[19]A. Bohr and B. R. Mottleson, *Nuclear Structure* (Benjamin, New York, 1969), Vol. I, pp. 152–158 and 281–293; *ibid.* (Benjamin, Reading, Mass., 1975), Vol. II, pp. 38–44, 591–636, and 654–666.
[20]S. E. Vigdor and H. J. Karwowski, Phys. Rev. C **26**, 1068 (1982).
[21]F. Puhlhofer, Nucl. Phys. **A280**, 267 (1977).
[22]L. McFadden and R. G. Satchler, Nucl. Phys. **84**, 177 (1966); F. G. Perey, Phys. Rev. **131**, 745 (1963).
[23]W. Dilg, W. Schantl, H. Vonach, and M. Uhl, Nucl. Phys. **A217**, 269, (1973).
[24]M. G. Mustafa, private communication.
[25]M. A. McMahan and J. M. Alexander, Phys. Rev. C **21**, 1261, (1980).
[26]A. Budzanowski, in *Proceedings of the Workshop on Coincident Particle Emission from Continuum States in Nuclei,* Bad Honnef, 1984, edited by H. Machner and P. Jahn (World Scientific, Singapore, 1985), p. 28.
[27]D. J. Moses, M. Kaplan, J. M. Alexander, D. Logan, M. Kildir, L. C. Vaz, N. N. Ajitanand, E. Duek, and M. S. Zisman, Z. Phys. A **320**, 229 (1985).
[28]L. C. Vaz and J. M. Alexander, Z. Phys. **318**, 231 (1984).
[29]G. La Rana, D. J. Moses, W. E. Parker, M. Kaplan, D. Logan, R. Lacey, J. M. Alexander, and R. J. Welberry, U.S. Department of Energy Report C00-3246-26, 1986 (unpublished).